NEUROIMAGING

White matter changes linked to visual recovery after nerve decompression

David A. Paul,[1,2] Elon Gaffin-Cahn,[1] Eric B. Hintz,[1,3] Giscard J. Adeclat,[4] Tong Zhu,[5] Zoë R. Williams,[6] G. Edward Vates,[3] Bradford Z. Mahon[1,3,7]*

The relationship between the integrity of white matter tracts and cortical function in the human brain remains poorly understood. We investigate reversible white matter injury, in this case patients with compression of the optic chiasm by pituitary gland tumors, to study the structural and functional changes that attend spontaneous recovery of cortical function and visual abilities after surgical removal of the tumor and subsequent decompression of the nerves. We show that compression of the optic chiasm led to demyelination of the optic tracts, which reversed as quickly as 4 weeks after nerve decompression. Furthermore, variability across patients in the severity of demyelination in the optic tracts predicted visual ability and functional activity in early cortical visual areas. Preoperative measurements of myelination in the optic tracts predicted the magnitude of visual recovery after surgery. These data indicate that rapid regeneration of myelin in the human brain is a component of the normalization of cortical activity, and ultimately the recovery of sensory and cognitive function, after nerve decompression. More generally, our findings demonstrate the use of diffusion tensor imaging as an in vivo measure of myelination in the human brain.

INTRODUCTION

Delayed axonal degeneration (*1*, *2*) describes a process of slow white matter injury that, if left unchecked, culminates in neuronal cell death. Despite the ubiquity of delayed axonal degeneration in humans, its impact on cortical function and cognitive performance is poorly understood. This is because delayed axonal degeneration is mediated by diffuse patterns of dysfunction in neuronal-glial biology, including demyelination (*3*), impaired axonal transport (*4*), and glutamate excitotoxicity (*5*). Also, white matter tracts with well-defined functional roles are difficult to isolate in the human brain. Consequently, we do not have prognostic biomarkers that are able to predict whether cortical activation and cognitive function will recover to normal levels after white matter injury. Here, we demonstrate the use of a specific disease model in humans—compression of the retinofugal nerve fibers by large pituitary tumors (*6*)—to characterize the relations between structural integrity of specific white matter tracts, cortical function, and vision. Figure 1 demonstrates the normal morphology of the pituitary gland and its placement relative to the optic chiasm, and also shows several examples of pituitary tumors compressing the optic chiasm. Patients with large pituitary tumors often experience a characteristic loss of vision in the temporal hemifields and decreased contrast sensitivity (CS) (*6*, *7*) due to selective compression of retinofugal fibers at the level of the optic chiasm (*8*). Surgical removal of the tumor and, thus, decompression of the optic chiasm is the most common treatment (*9*), with most patients (that is, 80 to 90%) experiencing some level of visual recovery after surgery. There is, however, substantial patient-to-patient variability in both the initial distribution of visual impairments across the visual field and the degree of recovery, which cannot be explained by tumor size (*10*), patient age (*11*), or preoperative visual examination (*12*).

Past research suggests that demyelination contributes to delayed axonal degeneration after optic nerve compression (*13*, *14*), although it is not clear how those processes alter early visual cortex function during the injured state and ultimately resolve to restore visual ability. One view is that improvement of secondary processes such as microtubule reorganization, axonal swelling, and ion channel permeability is responsible for early visual recovery (*14*, *15*). Another view is that remyelination plays an important role in supporting rapid recovery of visual abilities (*13*). An important observation in animal models is that partial remyelination can occur in as little as 2 to 4 weeks after a demyelinating event (*16*). However, it is not clear if remyelination occurs within the same time frame in the human brain, and if so, whether remyelination in the optic tracts is related to striate cortex function and ultimately the recovery of visual ability. Whereas the use of functional magnetic resonance imaging (fMRI) and psychophysics (that is, the quantitative measurement of visual ability) to study the primate visual system is well established (*17*–*22*), there is only one study on pituitary tumor patients using fMRI—a case study documenting both transient loss of visual ability and disruption of striate cortex (V1) activity after nerve compression by the pituitary tumor (*23*). Critically, that study was able to show that the pattern and magnitude of early visual cortex activation were directly related to the degree of visual field recovery, indicating a direct relationship between the reafferentation of early visual cortex and visual abilities in patients undergoing removal of pituitary tumors.

Here, we studied delayed axonal degeneration using diffusion tensor imaging (DTI) measurements made in cross section along the length of the optic tracts from the chiasm to the lateral geniculate nucleus (LGN). We calculated diffusion along both the principal (axial diffusivity) and perpendicular (radial diffusivity) axes. The average of these two measures estimates total diffusion in all directions [mean diffusivity (MD)], and the weighted variance [fractional anisotropy (FA)] provides a measure of how strongly diffusion occurs in the principal

[1]Department of Brain and Cognitive Sciences, University of Rochester, Rochester, NY 14642, USA. [2]Department of Neurobiology and Anatomy, University of Rochester School of Medicine, Rochester, NY 14642, USA. [3]Department of Neurosurgery, University of Rochester School of Medicine, Rochester, NY 14642, USA. [4]Department of Neuroscience, University of Rochester, Rochester, NY 14642, USA. [5]Department of Radiation Oncology, University of Michigan Medical Center, Ann Arbor, MI 48109, USA. [6]Department of Ophthalmology, University of Rochester School of Medicine, Rochester, NY 14642, USA. [7]Center for Visual Science, University of Rochester, Rochester, NY 14642, USA.
*Corresponding author. E-mail: mahon@rcbi.rochester.edu

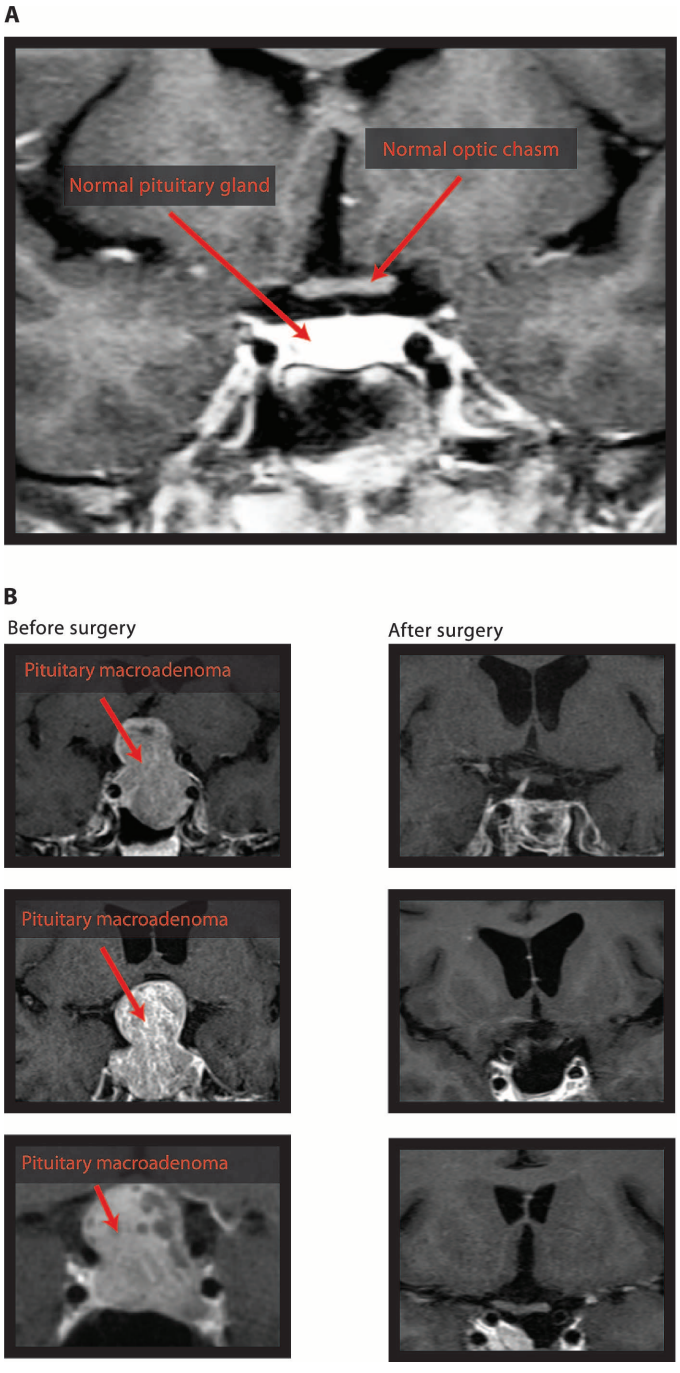

Fig. 1. Pituitary macroadenomas. (**A**) Coronal T1-weighted MRI with contrast at the level of the optic chiasm in a healthy participant showing the normal morphology of the pituitary gland and its relationship to the anterior visual pathway. (**B**) Coronal T1 MRIs with contrast for three compressive macroadenoma patients. In all three cases, the tumor displays marked suprasellar extension (that is, substantial tumor growth above the sella turcica, an osseous cave of the sphenoid bone along the base of the brain that houses the pituitary gland) and consequent upward displacement of the optic chiasm.

direction (*24*). Previous work in the mouse optic nerve shows that decreased labeling of myelin basic protein after retinal ischemia is associated with an increase in radial diffusivity (*25*). Thus, radial diffusivity may be used as an in vivo proxy for myelin integrity. Specifically, an increase in radial diffusivity that is disproportionate to changes in axial diffusivity is the signature of a breakdown in the myelin sheath (*26*, *27*). Using radial diffusivity as an in vivo measure of myelin integrity before and after surgical decompression of the optic chiasm, we show that (i) remyelination occurs in the human optic tract within 4 weeks of surgical decompression of retinofugal fibers, (ii) the degree of myelination of the optic tract is linked to normalization of retinotopic cortical function and visual abilities across patients, and (iii) preoperative DTI measurements of myelination predict substantial variability in visual recovery across patients.

RESULTS

We studied nine patients with compressive pituitary tumors before and after surgical tumor removal, as well as five patients with noncompressive pituitary tumors, and nine healthy control participants. Patients were tested with DTI, fMRI, and psychophysics both before and after surgery, and all post-surgery testing occurred within 4 weeks of surgery. Noncompressive control patients completed the same battery of tests, but only before surgery. All controls completed DTI and visual psychophysics (see Materials and Methods and the Supplementary Materials for details).

Psychophysical measurements are used to characterize visual abilities

Visual field mapping. Patients with compressive pituitary tumors demonstrated severe visual field deficits before surgery, primarily in the temporal hemifields (Fig. 2, A and B). Within 4 weeks of surgery, visual fields markedly improved for 71.4% of all hemifields tested, consistent with previous research (*11*) (see fig. S6 for individual patient data). Two key findings emerged from the visual field data. First, compared with all other participant groups, compressive pituitary tumor patients exhibited significantly reduced visual fields (mean = 0.629 ± 0.0785, significant at Bonferroni-corrected levels, $P < 0.0083$; Fig. 2C), which markedly recovered after surgery (mean = 0.881 ± 0.0315, $P < 0.006$). Second, visual fields in participants with noncompressive pituitary tumors were not significantly different from healthy controls ($P = 0.993$; Fig. 2C).

Contrast sensitivity. Compared with all other participant groups, individuals with compressive pituitary tumors (before surgery) exhibited decreased CS thresholds at all spatial frequencies tested (temporally stable stimuli; Fig. 2, D and F). Figure 2E displays the average full CS function for each participant group. We quantified the area under the log CS function (AULCSF) (*21*), weighted for each hemifield as was done for visual fields (see fig. S1). Analysis of AULCSF (see Fig. 2F) confirmed that patients with compressive pituitary tumors exhibited reduced CS (mean = 1.021 ± 0.122, significant at Bonferroni-corrected levels, $P < 0.0083$) compared to healthy control participants (mean = 1.80 ± 0.0765, $P < 0.003$) and compared to noncompressive pituitary tumor patients (mean = 1.640 ± 0.0957, $P < 0.0015$). In contrast to the marked postoperative improvements observed for visual fields, surgical decompression led to only moderate recovery of CS. After surgical decompression of the optic chiasm, 62.5% of hemifields showed increased CS 2 to 4 weeks after decompression (see fig. S6 for individual patient data). CS for noncompressive pituitary tumor patients was numerically lower, but not significantly different from control levels ($P = 0.882$; Fig. 2F).

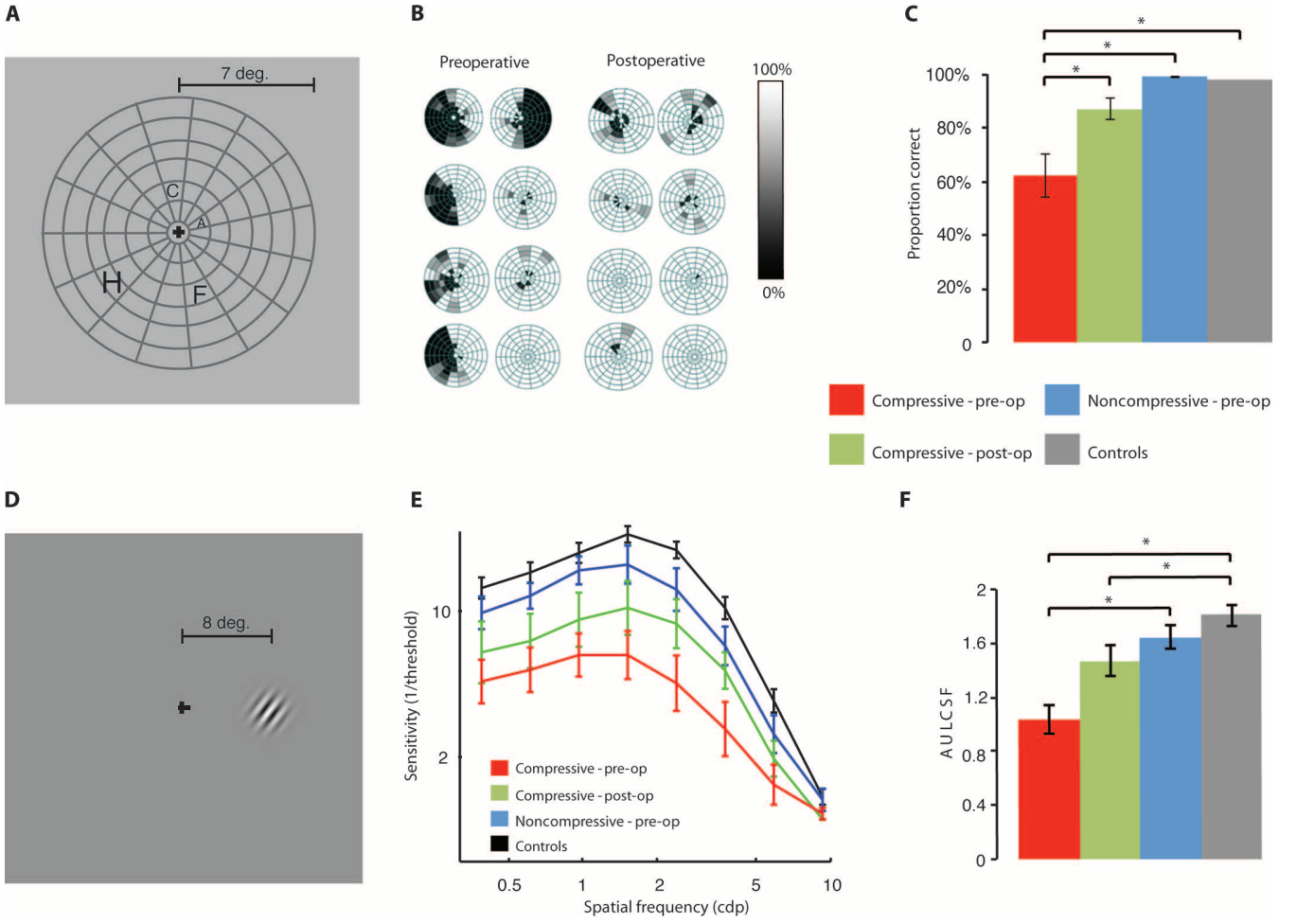

Fig. 2. Visual psychophysics tests. All psychophysical tests were completed one eye at a time, with the other eye patched. (**A** to **C**) Visual fields testing. (**D** to **F**) Contrast sensitivity. (A) Examples of stimuli used to assess visual fields. On each trial, a single letter was presented. (B) Visual fields, represented as percent correct letter identification, for a sample of compressive pituitary tumor patients, before and after surgery. The raw data were spatially (Gaussian) smoothed. (C) Visual fields were significantly reduced for preoperative compressive pituitary tumor patients ($P < 0.0083$, Bonferroni-corrected) and recovered with surgical tumor removal. Visual fields for noncompressive pituitary tumor patients were not different from healthy control participants [*$P < 0.0083$, one-way analysis of variance (ANOVA), and corresponding to Bonferroni correction at $P < 0.05$]. (D) Participants were tested using Gabor patches that orthogonally varied spatial frequency [up to 10 cycles per degree visual angle (cpd)] and contrast (stable stimuli, presented 8° to the right or left of fixation). (E) The mean CS function for each participant group is shown; error bars represent SEM over subjects. (F) CS, represented by the AULCSF (see fig. S2), was reduced before surgery compared with healthy controls ($P < 0.0083$, Bonferroni-corrected) but, unlike visual fields, did not return to healthy control values after surgery ($P < 0.0083$, Bonferroni-corrected). Noncompressive pituitary tumor patients were not significantly different than healthy control participants (*$P < 0.0083$, one-way ANOVA, and corresponding to Bonferroni correction at $P < 0.05$).

DTI is used to measure the structural integrity of nerve fibers

Figure 3 shows the diffusion measurements within each segment of the optic tract for patients and controls. The threshold for significant findings was set at the Bonferroni-corrected α level of $P < 0.0083$. The key finding was that increased radial diffusivity, computed across all segments in both optic tracts (mean = $1.38 \times 10^{-3} \pm 0.048 \times 10^{-3}$ mm^2/s) was the primary pathological change in the preoperative period for compressive pituitary tumor patients compared with healthy controls ($1.05 \times 10^{-3} \pm 0.24 \times 10^{-3}$ mm^2/s, significant at a Bonferroni-corrected $P < 0.0083$). Increased preoperative radial diffusivity in compressive pituitary tumor patients contributed to the observed changes in the other diffusion measurements, including reduced FA (0.24 ± 0.004) and increased MD ($1.57 \times 10^{-3} \pm 0.054 \times 10^{-3}$ mm^2/s; noncompressive tumor patients: FA, 0.345 ± 0.09; MD, $1.21 \times 10^{-3} \pm 0.26 \times 10^{-3}$ mm^2/s; healthy controls: FA, 0.35 ± 0.08; MD, $1.30 \times 10^{-3} \pm 0.26 \times 10^{-3}$ mm^2/s; comparing compressive patients to controls, all P values <0.0083). However, and critically, diffusion along the principal axis (axial diffusivity) of the optic tracts was not significantly different in patients with tumors compressing the nerve fibers ($1.96 \times 10^{-3} \pm 0.069 \times 10^{-3}$ mm^2/s) compared to healthy controls ($1.80 \times 10^{-3} \pm 0.20 \times 10^{3}$ mm^2/s; $P = 0.87$).

These data demonstrate a uniform pattern of increased radial diffusivity with spared diffusion along the principal axis in compressive pituitary tumor patients. This is in agreement with previous histological work in animal models that showed myelin disruption after axonal compression (*13*, *14*), as well as combined DTI-histological studies of isolated and reversible demyelinating lesions in mice (*26*). Individuals

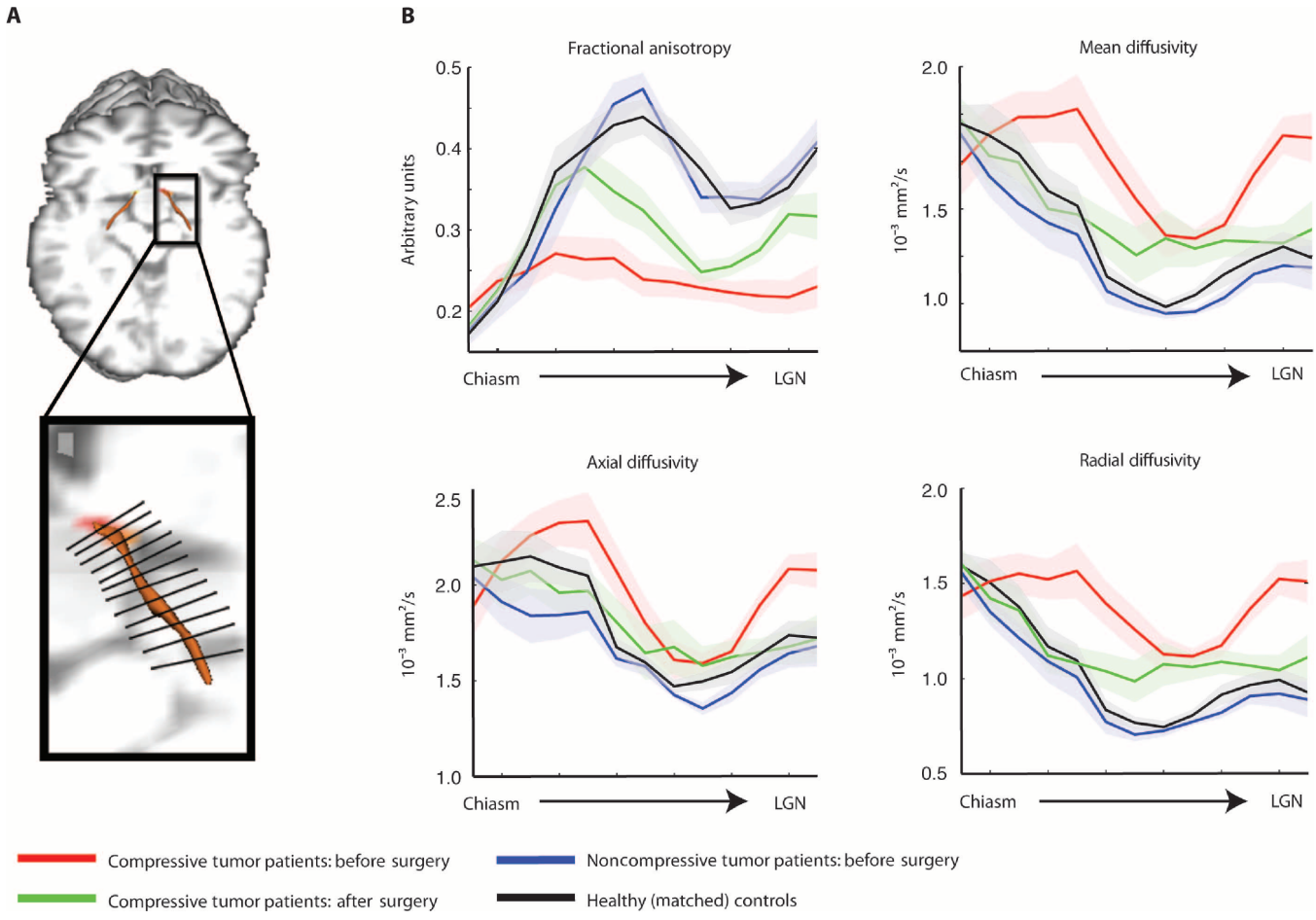

Fig. 3. Along-tract analysis of diffusion indices. (**A**) Schematic illustration of a segmented optic tract into 13 equidistant bins from the chiasm to the LGN using the along-tract statistics algorithm implemented in this study [for the basis of this approach, see (*46*); for all details, see the Supplementary Materials and fig. S4]. (**B**) Measures of diffusion (FA, MD, axial diffusivity, and radial diffusivity) were extracted from each segment, for each participant, and were plotted by segment position within each group. The shaded region around each line represents the SEM (over participants). The consistent pattern of variability in diffusion measurements, for all participant groups, along the length of the optic tract results from the proximity of the optic tracts to major fiber bundles, particularly the corticospinal tracts. This observation is in line with previous studies of the optic tracts (*47*) and other white matter fiber bundles (*44*).

with noncompressive tumors (that is, patient controls) demonstrated patterns of diffusion measurements that were equivalent to healthy control participants, indicating that the demyelination observed in the critical patients was directly tied to the tumor compression.

After surgery, 13 of 14 optic tracts in compressive pituitary tumor patients showed normalization in FA, MD, and radial diffusivity (see fig. S7 for an outlier analysis of the one tract that did not recover). A numerical (but statistically nonsignificant) trend was observed for axial diffusivity, in which 10 of 14 optic tracts demonstrated reduced axial diffusivity after surgery. Whereas the diffusion indices largely resolved during the early phase of recovery (within 1 month after surgery), they did not fully return to healthy control values. Figure 3 shows that anterior and posterior optic tract segments are more likely to demonstrate rapidly improved diffusion indices (see table S1 for a complete list of all diffusion indices in both the right and left optic tracts of all participants enrolled in the study).

Relation between myelination of the optic tracts and visual ability

We then tested whether variability across patients in myelination of the optic tracts, as measured with radial diffusivity, predicted visual abilities. This analysis is illustrated in Fig. 4 using a matrix of Pearson's Rho values for the correlation across patients between DTI indices in each optic tract segment and visual field performance (Fig. 4A) and CS (Fig. 4B). Higher levels of FA were associated with better visual abilities (positive Rho values), whereas higher levels of MD and radial diffusivity were associated with worse visual abilities (negative Rho values). There was little, if any, relationship between axial diffusivity and visual abilities. This pattern indicates that the key microstructural property in the optic tracts that is related to visual performance is the level of myelination. This also means that the relationships between visual abilities and MD and FA were secondary to variability in radial diffusivity.

To evaluate whether the observed relationship between radial diffusivity and visual abilities was in fact driven by surgical decompression of the optic chiasm, we correlated the change in diffusivity indices with the change in visual abilities for the subset of patients with compressive tumors in whom we had both pre- and postoperative DTI and visual fields data ($n = 6$). This analysis computed difference scores (postoperative minus preoperative) across each segment of the optic tract for every subject, for the four DTI measures, as well as the postoperative

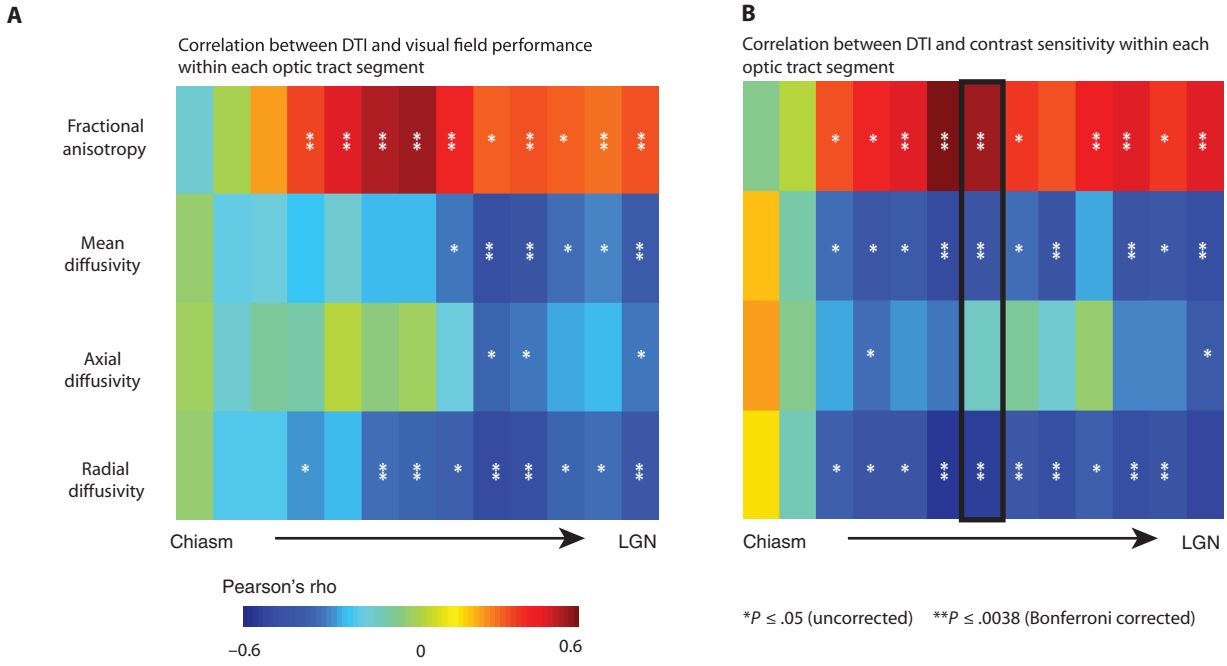

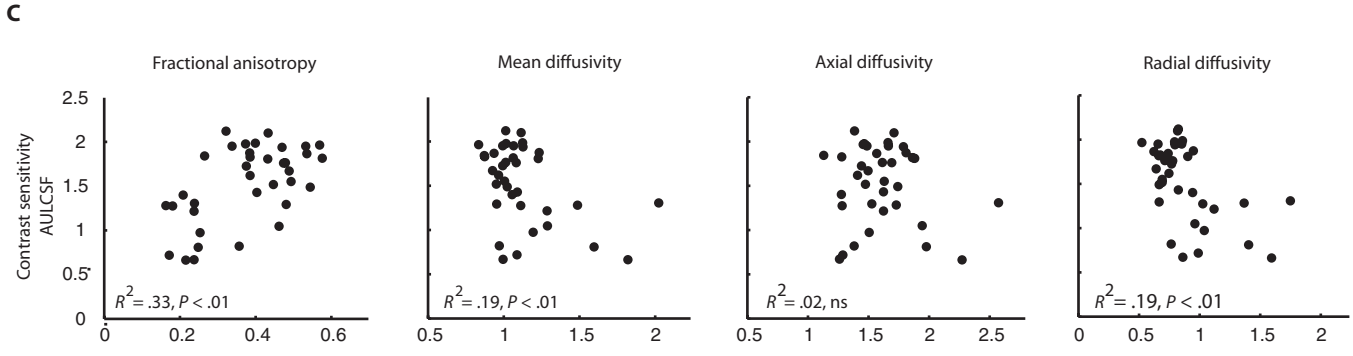

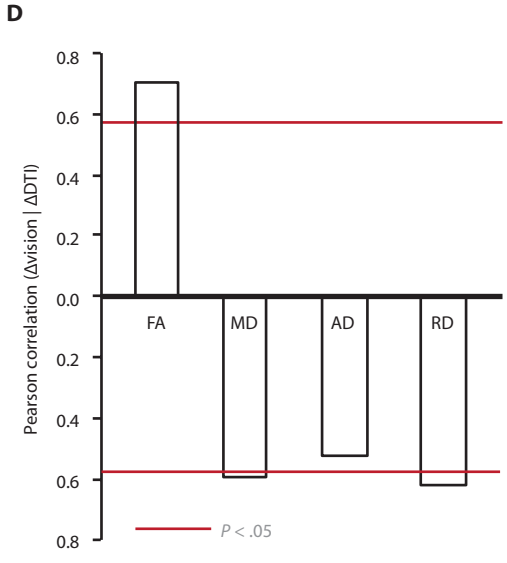

Fig. 4. Relation between diffusion indices and visual ability. (**A** and **B**) Within each segment of the optic tract, variability across all patients in diffusion indices was correlated with variability in (A) visual fields and (B) AULCSF. Diffusion indices from a given optic tract (for example, right optic tract) were correlated with psychophysical data from the contralateral visual field (that is, left visual hemifield of both eyes). Whereas no relationships were observed between axial diffusivity and visual ability, radial diffusivity was negatively correlated with visual abilities. Near the optic chiasm (that is, the first two segments), correlations were consistently poor for all diffusion indices, likely due to artifacts from crossing retinofugal axons at the chiasm (*$P < 0.05$, uncorrected; **$P < 0.0083$, Bonferroni-corrected). (**C**) Diffusivity values from the middle segment of the optic tract (segment 7) are plotted against AULCSF. ns, not significant. (**D**) Summary of the correlation between the change in diffusivity measurements in the optic tract and the change in visual abilities as a function of surgery. AD, axial diffusivity; RD, radial diffusivity.

minus preoperative difference in visual abilities. The resulting Pearson's Rho (r) values (Fig. 4D) describing the relation between difference scores of DTI indices (averaged over all segments of the optic tract) and visual abilities confirmed the pattern observed in the cross-sectional analyses. There was a relationship between radial diffusivity and visual fields (average $r = -0.62$, $P < 0.05$), and a weaker pattern for axial diffusivity (average $r = -0.52$, $P = 0.09$). There were also significant relationships between FA (average $r = 0.71$, $P < 0.05$) and MD (average $r = 0.59$, $P < 0.05$) and visual fields. Finally, the relation between radial diffusivity and visual abilities was stronger than the relation between axial diffusivity and visual abilities (t test, two-tailed, over Fisher-transformed r values across all segments in the optic tract: $t_{11} = 2.56$, $P < 0.05$). The same dissociation between radial and axial diffusivity was present when the analysis was repeated over Fisher-transformed Spearman rank-ordered correlation coefficients, ruling out a contribution from outlier data points ($t_{11} = 2.56$, $P < 0.05$).

In summary, regardless of whether the relationship between diffusion indices and visual abilities is carried out in a cross-sectional manner (Fig. 4, A to C) or within patient in a longitudinal manner (Fig. 4D), radial diffusivity explains more variance in visual abilities than does axial diffusivity.

Relation between diffusivity indices in the optic tracts and cortical retinotopic activity

If the degree of myelination in the optic tracts and visual abilities is in fact specifically related to the cascade of pathologies induced by compression of the early visual system, there should also be a relation between diffusion indices and the pattern of retinotopic activation in early visual areas. Figure 5A displays retinotopic cortical activity in the right occipital lobe of a representative compressive pituitary tumor patient before and after surgery. Those data represent a replication of the findings of Chouinard and colleagues (*23*). Our principal interest was not in whether there was deformation of the retinotopic map (*28*, *29*), but to use fMRI signal reproducibility in early visual areas as an objective and implicit measure of visual function. Thus, the fidelity of retinotopic preferences was calculated using linear correlation over multivoxel patterns (*30*). This analysis correlated voxel-wise patterns, over β values coding retinotopic preferences, between even and odd revolutions of the wedge within a run of polar angle mapping (for details, see Materials and Methods and fig. S5). To ensure that we could replicate the findings of Chouinard and colleagues (*23*) using this new approach, we correlated the variability in the resulting r values across participants (by quadrant) to visual field maps (for the respective quadrants)—the results indicated a relationship between visual fields and fMRI signal reproducibility ($r = 0.66$, $P < 0.01$). That relationship both extends the observations of Chouinard and colleagues (*23*) to an across-subject analysis, and validates this approach for using BOLD signal in striate cortex as an implicit measure of visual function.

We then tested whether variability across patients in fMRI signal reproducibility was related to variability in diffusivity indices, for each segment of the optic tract. In Fig. 5C, MD, axial diffusivity, and radial diffusivity were all strongly predictive of fMRI signal reproducibility—with increased diffusivity values corresponding to decreased retinotopic activation. These data reveal an important dissociation: both axial diffusivity and radial diffusivity are related to fMRI signal reproducibility in striatal cortex (Fig. 5C), and fMRI signal reproducibility in striatal cortex is related to visual ability (Fig. 5B); however, only radial diffusivity is directly related to visual ability (Fig. 4). This dissociation confirms that axial diffusivity and radial diffusivity are indexing distinct, and functionally relevant, structural properties of nerve fibers.

Presurgical DTI predicts visual recovery

Given the tight relationship between diffusion measurements of the optic tracts and visual abilities across the group of patients, a question of great clinical significance is whether it is possible to predict the degree of visual recovery (that is, postoperative minus preoperative visual fields) based only on preoperative DTI data. From our data set, we had pre- and postoperative visual fields data as well as preoperative DTI data in six patients (that is, 12 hemispheres). We took two approaches—linear correlation and support vector regression—to test whether preoperative diffusion indices predict the change in visual abilities (that is, visual field performance) as a function of surgery.

In the first analysis, we correlated preoperative diffusivity indices for each segment of the optic tract with the change in visual abilities, across participants. The resulting correlation coefficients, averaged across all segments of the optic tracts, indicated that preoperative radial diffusivity was significantly related to improvement in visual abilities (average $r \pm$ SEM over tract segments, one-sample t test over Fisher-transformed r values: $0.24 \pm .05$, $t_{11} = 4.7$, $P < 0.0006$). The corresponding analysis for axial diffusivity indicated only a marginally significant relationship between preoperative axial diffusivity and the change in visual abilities ($r = 0.12 \pm .06$, $t_{11} = 2.1$, $P = 0.06$). Because both FA and MD are derived from measures of radial and axial diffusivity, the corresponding analyses for those diffusivity indices were significant (FA: $r = -0.27 \pm .04$, $t_{11} = 6.8$, $P < .0001$; MD: $r = 0.21 \pm .05$, $t_{11} = 3.9$, $P < 0.003$). Finally, the relation between preoperative radial diffusivity and visual improvement was stronger than the relation between preoperative axial diffusivity and visual improvement (paired t test over Fisher-transformed values, two-tailed: $t_{11} = 4.8$, $P < 0.0005$).

In a second analysis, we used a machine-learning approach [support vector regression (SVR)] to test whether preoperative variability in diffusivity indices along the segments of the optic tract predicted postoperative visual outcome. The feature vectors for support vector training and testing consisted of the DTI indices along the segments of the optic tract, with each hemisphere in each patient constituting an observation. The significance of this approach, and what distinguishes it from the above approach based on linear correlation, is that SVR predicts a given hemisphere's visual outcome as a function of the preoperative DTI data for that hemisphere and support vectors that are trained on the other hemispheres in the data set (that is, jackknifed across all hemispheres in the data set).

We evaluated the reliability of the trained support vectors in two ways. First, we computed the linear correlation between predicted visual abilities and observed visual abilities, and from that, the explained variance (r^2). This analysis indicated that preoperative radial diffusivity predicted 49% of the variance in observed visual outcome ($P < 0.05$), whereas preoperative axial diffusivity predicted 17% of the variance in observed visual outcome ($P > 0.05$). Second, we used a Monte Carlo–style permutation test in which, on each of 100,000 iterations, the training data were randomly shuffled, and each of the 12 hemispheres individually tested (having trained the support vectors on the remaining 11 hemispheres; Fig. 6B). These permutation tests generated null distributions of r^2 values (that is, explained variance) for each of the four diffusivity indices. Plotted in each null distribution is the performance of the SVR model on unshuffled data (that is, from Fig. 6A). The results of these permutation tests indicated that preoperative

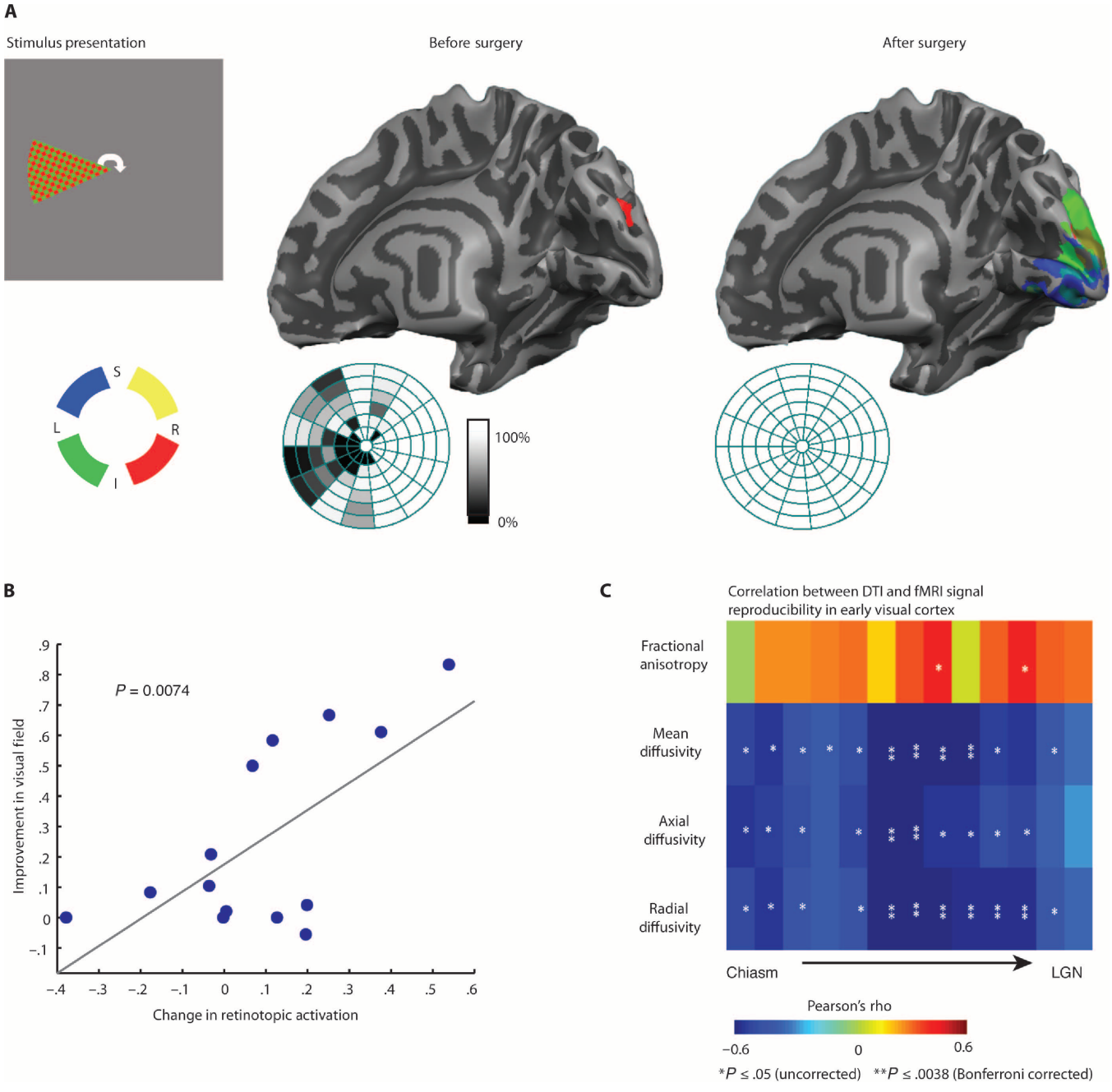

Fig. 5. Relation among DTI, visual fields, and retinotopic activity. (**A**) Example of visual field representations in early visual cortex in a single compressive pituitary tumor patient before and after surgery. Cortical responses in the right hemisphere normalized after surgery, whereas before surgery, the only activation was a small spot of ectopic activity from the ipsilateral stimulus. Also shown are the same individual's visual fields for the left eye (right eye patched during scanning). (**B**) The scatter plot shows the effect of surgical decompression of the early visual pathway on visual fields and retinotopic activity for corresponding quadrants. (**C**) Relationships between diffusion indices for each segment of the optic tract and retinotopic information content, displayed as a matrix of *r* values (*$P < 0.05$, uncorrected; **$P < 0.0083$, Bonferroni-corrected).

radial diffusivity predicted visual recovery better than 98.7% of the null distribution (that is, bootstrapped $P < 0.014$), whereas preoperative axial diffusivity predicted visual recovery better than 81.5% of the null distribution (bootstrapped $P = 0.185$). Preoperative FA predicted visual recovery better than 98.3% of the null distribution (bootstrapped $P < 0.018$), whereas preoperative MD predicted visual recovery better than 93.2% of the null distribution (bootstrapped $P = 0.068$; null distributions for FA and MD not shown in Fig. 6).

Together, there is a dissociation between the ability of preoperative radial and axial diffusivity to predict visual recovery: preoperative radial diffusivity is significantly correlated across patients with the change in visual abilities and predicts a substantial portion of variance

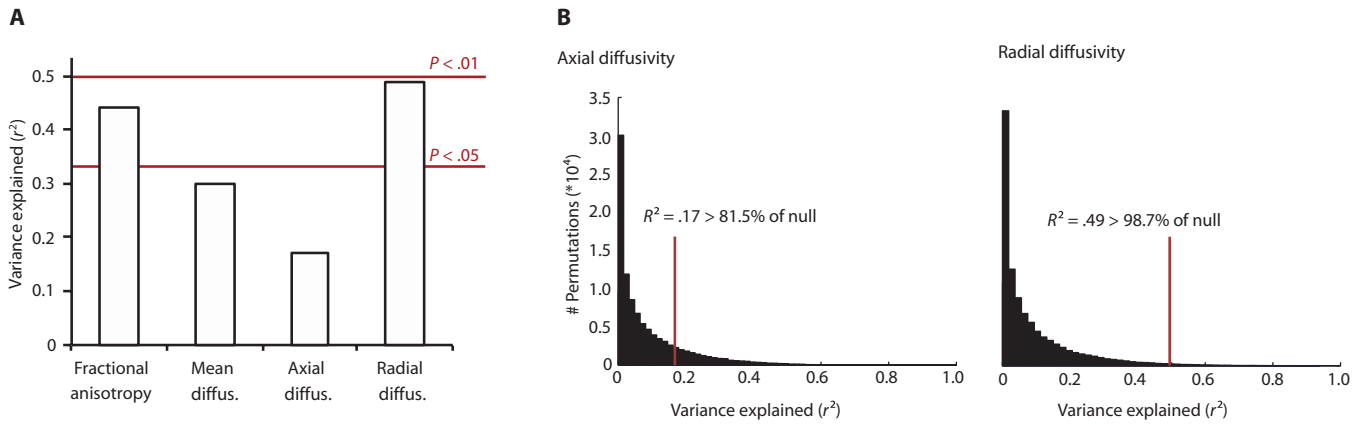

Fig. 6. Preoperative diffusivity along the optic tract predicts visual recovery. An SVR (linear kernel) model was trained on the along-tract diffusivity indices, separately for each of the four diffusivity measurements. The support vectors were trained on 11 hemispheres and then tested on the 12th hemisphere. The analysis was jackknifed across the 12 hemispheres, each time leaving one out for test and training on the remaining 11. (**A**) The graph plots explained variance in visual recovery across all hemispheres in the sample; whereas support vectors trained on along-tract measurements of radial diffusivity could predict 49% of the variance in the observed data, equivalent analyses with axial diffusivity predicted (a nonsignificant) 17% of the variance. (**B**) Null distributions were bootstrapped using permutation tests over randomly shuffled data; histogram plot explained variance (r^2) for permutations over axial and radial diffusivity data. The vertical red line indicates the performance of the model on unshuffled data [from (A)], and written percentages indicate where model performance fell along the bootstrapped null distribution.

in visual outcome (49%), whereas axial diffusivity is, at best, weakly correlated with the change in visual abilities and predicts only a modest (and nonsignificant) amount of variance in visual outcome (17%).

DISCUSSION

Compression of the optic chiasm by large pituitary tumors is a disease model that permits in vivo and longitudinal analysis of the effects of nerve crush injury on white matter tracts in the human brain. Surgical removal of the tumors and subsequent decompression of the early visual pathway have long been known to be associated with a staged return of visual abilities. Here, we found that demyelination of the optic tracts is a key aspect of white matter injury caused by pressure block injury in the brain, and that substantial remyelination occurs within 4 weeks of surgical decompression. Furthermore, the degree of myelination across patients is directly related to visual ability, and preoperative measurements of myelination in the optic tracts predict nearly half of the variance in visual recovery. These findings demonstrate the speed of remyelinating processes in the central nervous system in humans and show that those regenerative processes are the driving force behind the rapid recovery of visual abilities that follow surgical decompression of the early visual pathway. These data also indicate that preoperative measurements provide a basis for predicting a substantial portion of variability in visual recovery, and more generally support the use of radial diffusivity as an in vivo measure of myelination in the human brain.

As previously discussed, an important precedent for the current investigation are combined DTI-histological studies in animal models that collectively support the connection between radial diffusivity and myelin integrity across a wide range of experimentally induced pathologies, including retinal ischemia (*25*), cuprizone-mediated demyelination (*26*), transgenic shiverer mice (*27*), dorsal root axotomy (*31*), and Wallerian degeneration (*32*). An increase in radial diffusivity that is both disproportionate to changes in axial diffusivity and consistent with the direction of the principal eigenvector (*33*) is an indication of decreased myelination. Similarly, a reduction in radial diffusivity independent of changes in axial diffusivity (*26*) is associated with remyelination. This has been demonstrated with decreased radial diffusivity after injection of human oligodendrocyte precursor stem cells into patients with a rare hypomyelinating genetic disorder, Pelizaeus-Merzbacher disease (*34*). We were able to ensure the uniformity of the principal eigenvector across subjects by implementing a probabilistic tractography approach (see Materials and Methods and the Supplementary Materials for details). It is also important to note that an increase in radial diffusivity preoperatively, followed by a decrease in axial diffusivity, would be suggestive of severe axonal damage, often expressed as either Wallerian degeneration or late-stage tissue ischemia (*25*). However, because in the present study axial diffusivity remained stable across the cohort of compressive pituitary tumor patients, it is not likely that Wallerian degeneration or tissue ischemia played a significant role in these patients with pressure block injury to the early visual pathways. Rapid remyelination from 0 to 4 weeks after nerve decompression satisfies both the anatomic and physiologic requirements of a functionally significant reduction in radial diffusivity (*4*, *35*). This conclusion is consistent with the findings of Naismith and colleagues (*36*), who found that radial diffusivity in the optic nerves strongly correlated with both visual evoked potential (VEP) conduction velocity (an indirect measure of myelination), and severity of vision loss at about 6 months after a remote episode of optic neuritis (*36*).

To date, one of the difficulties associated with the diagnosis of secondary white matter injury, and thus an important obstacle for developing prognostic indicators and measuring the efficacy of new therapeutics, is that it has not been clear what combination of DTI indices should be tested. Patients with pituitary tumors offer a new model for understanding both the process of spontaneous remyelination in the human brain and the functional consequences of that remyelination, and therefore provide new opportunities to develop indicators for secondary white matter injury. This is important because, as noted above, there have been notable failures to predict the likelihood of visual recovery after decompression of retinofugal nerves: factors such as

tumor size, duration of compression, severity of presurgical visual impairments, and age do not predict visual outcome (*10*–*12*). Previous neuro-ophthalmological research on macroadenoma patients (*15*, *37*) using pattern electroretinography (PERG), photopic negative response (PhNR), and retinal nerve fiber layer (RNFL) thickness has found that PERG can predict only failure of visual recovery (*38*), whereas postoperative PhNR and RNFL thickness correlate with visual field outcomes at 3 to 6 months (*15*). However, PhNR and RNFL thickness do not increase during the early phase of visual recovery, that is, within the time frame of the current study (*15*). Increased visual ability in the absence of a corresponding increase in RNFL and PhNR values during the early phase of recovery supports the notion that retinal ganglion cell health cannot be the complete story behind improved visual outcomes.

DTI presents several advantages over other available techniques, such as VEP- and optical coherence tomography (OCT)–based measurements of RNFL. First, we have established a role for radial diffusivity in the assessment of subtle structural changes to the visual system that cannot be measured using PhNR or RNFL. It should be noted though that there is likely to be a threshold or cutoff on the predictive use of radial diffusivity, as is the case for RNFL, beyond which irreparable damage to the axons has occurred and visual recovery is not feasible. However, importantly, this means that radial diffusivity provides a sensitive measure with which to assess subtle changes that may not be detectable with RNFL. Further studies relating diffusion measurements, particularly axial diffusivity, with RNFL in healthy individuals and across a broad range of ophthalmological diseases are needed to establish the relation between diffusion indices and ganglion cell anatomy in the human visual pathways. Furthermore, combining RNFL, DTI, and VEPs in longitudinal assessments of patients undergoing chiasmatic decompression offers a promising approach toward developing a comprehensive suite of noninvasive in vivo markers for myelination with general application.

A second advantage of DTI over other approaches for assessing myelination of nerve fibers is that it provides a means to study the structural integrity of isolated white matter tracts, and even isolated segments of specific white matter tracts, independent of their function. This is important because although it is possible to study the function of the retinofugal nerve pathway (using retinotopic fMRI and visual psychophysics), this is often not feasible for major white matter pathways that link high-level cortical regions in the brain. With DTI, we have shown that it is possible to identify the diffusion-related changes that lead to functional impairments before neuronal cell death, and to identify the structural changes that facilitate functional recovery. This offers a new means with which to directly measure the efficacy of new therapies designed to promote the regeneration of myelin in the human brain (*39*).

MATERIALS AND METHODS

Study design

The objective of this study was to understand the role of myelin regeneration during the initial period (first 2 to 4 weeks) of visual recovery after decompression of the optic chiasm in patients with compressive pituitary tumors—in particular, the relationship between myelination, visual abilities, and striate cortex activation. Patients (see below for recruitment information) were studied in a prospective longitudinal fashion and evaluated both before and after surgical tumor removal. DTI was used to evaluate the structural integrity of the optic tracts, with radial diffusivity as a marker of myelination. Visual psychophysics and fMRI were used to study visual ability and striate cortex activity, respectively.

Participant recruitment

Patients were recruited as part of an ongoing pituitary tumor research study approved by the Research Subjects Review Board at the University of Rochester. Individuals diagnosed with a pituitary or parasellar tumor without any confounding factors, including glaucoma, diabetic retinopathy, multiple sclerosis, stroke, or previous head trauma, between September 2012 and August 2013 are included in this study. Healthy controls ($n = 9$) were also recruited from the Rochester, NY, community and underwent the same battery of DTI and psychophysical testing as the patient group. Table S1 displays the demographic information for all study participants. All patients and healthy control subjects gave written informed consent (see the Supplementary Materials for additional participant information).

Assessment of visual psychophysics

Each participant was tested monocularly in both eyes, at a viewing distance of 50 cm (ViewSonic VX2265wm; resolution, 1680 × 1050; 120 Hz; average background luminance, 166 cd/m^2). Fixation was monitored using an EyeLink 1000 Eye Tracker. For visual field testing, high-contrast letters were presented (one per trial) 10 times the minimum size for recognition at different locations in the visual field (*40*), and participants verbally named the letters (see Fig. 2A). All letter stimuli were presented within 14° of a black fixation cross. CS thresholds were measured using a Bayesian algorithm that allows fast estimation of the CS curve (*21*). Each hemifield was tested for each eye using temporally stable stimuli (Gabor patches 3° in diameter) of varying spatial frequency, up to 10 cycles per degree. Stimuli were presented 8° to either the right or the left of a black fixation cross, and participants were asked to judge whether the stimulus was oriented 45° to the right or the left (see Fig. 2D for an example stimulus).

MRI acquisition parameters

All participants were scanned at the Rochester Center for Brain Imaging on a 3-T Siemens MAGNETOM Trio scanner with a 32-channel head coil. High-resolution sagittal T1-weighted anatomical images were acquired at the start of each session with a MPRAGE (magnetization-prepared rapid acquisition gradient echo) pulse sequence [repetition time (TR) = 2530 ms, echo time (TE) = 3.44 ms, flip angle = 7°, field of view (FOV) = 256 mm, matrix = 256 × 256, 1 × 1 × 1 mm]. DTI was acquired using a single-shot echo planar sequence (60 diffusion directions, TR/TE = 8900/86 ms, b = 1000 s/mm^2, 70 slices with resolution of 2 × 2 × 2 mm, 10 non–diffusion-weighted volumes). BOLD fMRI was obtained with an echo planar imaging pulse sequence (TR = 2000 ms, TE = 30 ms, flip angle = 90°, FOV = 256 mm, matrix 64 × 64, 30 sagittal left-to-right slices, isovoxel size 4 × 4 × 4 mm).

fMRI stimulus presentation

Cortical activation in early visual areas was elicited using a (clockwise) rotating wedge stimulus that subtended 21.6°, and consisted of a high-contrast green and red checkerboard pattern that flickered at 5 Hz and scaled with eccentricity. The wedge completed one rotation in 64 s and made eight clockwise rotations per functional run. Subjects were instructed to focus their gaze on a fixation cross located at the center of screen. Because of time limitations, it was possible to study only one eye in each participant (the other eye was patched). In all patients, we used

monocular performance on the visual field test before scanning to determine which eye had the most clearly compromised impairment that was specific to a region of the visual field.

Preprocessing of MRI data

DTI. Motion artifacts, eddy current distortions, and B0 distortions were reduced using the FMRIB (Functional Magnetic Resonance Imaging of the Brain) software library (FSL 4.1.8, www.fmrib.ox.ac.uk/fsl) (*41*). Probability distributions of fiber direction at each voxel (up to two per voxel) in the preprocessed DTI sets were calculated using Bayesian estimation of diffusion parameters (BEDPOSTX) in FSL. Additionally, each preprocessed DTI image was brain-extracted using BET, before image registration. The first non–diffusion-weighted ($b = 0$) volume in each subject was then registered to the corresponding skull-stripped T1-weighted image and the MNI152 template using a correlation ratio cost function and 6 degrees of freedom to define transformation matrices between the spaces.

Functional magnetic resonance imaging. The first two volumes of each run were discarded for signal equilibration. Preprocessing of fMRI data included slice time correction, three-dimensional motion correction aligned to the first run, and high-pass temporal filtering (more than two cycles per run) linear co-registration on a subject-by-subject basis to the deskulled T1 anatomical image, and conversion to standardized Talairach space. Preprocessing was performed with BrainVoyager QX batched with custom scripts.

Data analysis

DTI tractography. To isolate the optic tracts, we used probabilistic tractography—a Bayesian method for calculating the probability density functions of white matter connections in the brain (*42*). Because of the extremely small cross-sectional area of the optic tracts (*43*), 5.1 to 11.3 mm^2 and neighboring anteroposterior tract groups, a single-voxel seed mask was used to generate the tract profile (see the Supplementary Materials and fig. S3).

Along-tract statistics algorithm. Various along-tract statistics algorithms have been used previously to study white matter changes during development and in disease (*44*, *45*). Here, we use a novel approach loosely based on methods developed to analyze geospatial representations of river channels (*46*). Full details of this analysis can be found in the Supplementary Materials (see fig. S4).

Defining retinotopic information content in early visual cortex (fMRI). Retinotopically responsive voxels were identified for each hemifield separately, using phase-lag analysis (with the left half or the right half of the checkerboard sweep, as is standard). Each run was analyzed separately, and retinotopically responsive voxels were determined as those voxels that met or surpassed a threshold of $r > 0.30$ and fell within the bounds of an occipital lobe mask. To define the strength of retinotopic response to the visual stimuli, we ran a fixed-effects generalized linear model (GLM) (using a standard dual gamma HRF) for each run with predictors for each quadrant that excluded time points when the checkerboard stimulus was at the vertical or horizontal meridians, and separate predictors for even and odd revolutions of the wedge (that is, eight predictors per GLM). Refer to the Supplementary Materials and fig. S5 for details.

Statistics

All data are presented as means ± 1 SD unless stated otherwise. The MATLAB software package was used for all statistical analyses, and comparisons were Bonferroni-corrected at $P < 0.05$ for significance. Details of the individual statistical tests are provided in Supplementary Methods.

SUPPLEMENTARY MATERIALS

www.sciencetranslationalmedicine.org/cgi/content/full/6/266/266ra173/DC1
Methods
Fig. S1. Schematic of weighting of visual performance data by optic tract.
Fig. S2. Convergence of AULCSF by trial number for all participants.
Fig. S3. Demonstration of tractography of the optic tract in a patient with a pituitary macroadenoma.
Fig. S4. Schematic of along-tract statistics algorithm.
Fig. S5. Schematic of multivoxel linear correlation analysis (MVPA).
Fig. S6. Pre- and postoperative visual ability of each compressive pituitary tumor patient.
Fig. S7. Identification of data outlier using Mahalanobis distance.
Table S1. Demographic information of enrolled participants and tract averaged diffusion indices.
References (*48*–*51*)

REFERENCES AND NOTES

1. M. J. Crowe, J. C. Bresnahan, S. L. Shuman, J. N. Masters, M. S. Beattie, Apoptosis and delayed degeneration after spinal cord injury in rats and monkeys. *Nat. Med.* **3**, 73–76 (1997).
2. E. Yoles, M. Schwartz, Degeneration of spared axons following partial white matter lesion: Implications for optic nerve neuropathies. *Exp. Neurol.* **153**, 1–7 (1998).
3. M. O. Totoiu, H. S. Keirstead, Spinal cord injury is accompanied by chronic progressive demyelination. *J. Comp. Neurol.* **486**, 373–383 (2005).
4. W. L. Maxwell, D. I. Graham, Loss of axonal microtubules and neurofilaments after stretch-injury to guinea pig optic nerve fibers. *J. Neurotrauma* **14**, 603–614 (1997).
5. E. Park, A. A. Velumian, M. G. Fehlings, The role of excitotoxicity in secondary mechanisms of spinal cord injury: A review with an emphasis on the implications for white matter degeneration. *J. Neurotrauma* **21**, 754–774 (2004).
6. H. Cushing, C. B. Walker, Distortions of the visual fields in cases of brain tumor chiasmal lesions, with especial reference to bitemporal hemianopsia. *Brain* **37**, 341–400 (1915).
7. V. Porciatti, P. Ciavarella, M. R. Ghiggi, V. D'Angelo, S. Padovano, M. Grifa, G. Moretti, Losses of hemifield contrast sensitivity in patients with pituitary adenoma and normal visual acuity and visual field. *Clin. Neurophysiol.* **110**, 876–886 (1999).
8. G. Tassinari, C. Marzi, B. Lee, V. Di Lollo, D. Campara, A possible selective impairment of magnocellular function in compression of the anterior visual pathways. *Exp. Brain Res.* **127**, 391–401 (1999).
9. I. Ciric, M. Mikhael, T. Stafford, L. Lawson, R. Garces, Transsphenoidal microsurgery of pituitary macroadenomas with long-term follow-up results. *J. Neurosurg.* **59**, 395–401 (1983).
10. A. M. Tokumaru, I. Sakata, H. Terada, S. Kosuda, H. Nawashiro, M. Yoshii, Optic nerve hyperintensity on T2-weighted images among patients with pituitary macroadenoma: Correlation with visual impairment. *AJNR Am. J. Neuroradiol.* **27**, 250–254 (2006).
11. K. K. Gnanalingham, S. Bhattacharjee, R. Pennington, J. Ng, N. Mendoza, The time course of visual field recovery following transphenoidal surgery for pituitary adenomas: Predictive factors for a good outcome. *J. Neurol. Neurosurg. Psychiatry* **76**, 415–419 (2005).
12. A. G. Chacko, K. S. Babu, M. J. Chandy, Value of visual evoked potential monitoring during trans-sphenoidal pituitary surgery. *Br. J. Neurosurg.* **10**, 275–278 (1996).
13. R. E. Clifford-Jones, D. N. Landon, W. I. McDonald, Remyelination during optic nerve compression. *J. Neurol. Sci.* **46**, 239–243 (1980).
14. L. J. Cottee, C. Daniel, W. S. Loh, B. M. Harrison, W. Burke, Remyelination and recovery of conduction in cat optic nerve after demyelination by pressure. *Exp. Neurol.* **184**, 865–877 (2003).
15. C. H. Moon, S. C. Hwang, Y. H. Ohn, T. K. Park, The time course of visual field recovery and changes of retinal ganglion cells after optic chiasmal decompression. *Invest. Ophthalmol. Vis. Sci.* **52**, 7966–7973 (2011).
16. F. J. Sim, G. L. Hinks, R. J. M. Franklin, The re-expression of the homeodomain transcription factor Gtx during remyelination of experimentally induced demyelinating lesions in young and old rat brain. *Neuroscience* **100**, 131–139 (2000).
17. S. A. Engel, D. E. Rumelhart, B. A. Wandell, A. T. Lee, G. H. Glover, E. J. Chichilnisky, M. N. Shadlen, fMRI of human visual cortex. *Nature* **369**, 525 (1994).
18. S. A. Engel, G. H. Glover, B. A. Wandell, Retinotopic organization in human visual cortex and the spatial precision of functional MRI. *Cereb. Cortex* **7**, 181–192 (1997).
19. X. Jiang, E. Bradley, R. A. Rini, T. Zeffiro, J. Vanmeter, M. Riesenhuber, Categorization training results in shape- and category-selective human neural plasticity. *Neuron* **53**, 891–903 (2007).
20. C. S. Konen, M. Behrmann, M. Nishimura, S. Kastner, The functional neuroanatomy of object agnosia: A case study. *Neuron* **71**, 49–60 (2011).

21. L. A. Lesmes, Z. L. Lu, J. Baek, T. D. Albright, Bayesian adaptive estimation of the contrast sensitivity function: The quick CSF method. *J. Vis.* **10**, 17.1–21 (2010).
22. M. I. Sereno, A. M. Dale, J. B. Reppas, K. K. Kwong, J. W. Belliveau, T. J. Brady, B. R. Rosen, R. B. Tootell, Borders of multiple visual areas in humans revealed by functional magnetic resonance imaging. *Science* **268**, 889–893 (1995).
23. P. A. Chouinard, C. L. Striemer, W. H. Ryu, I. Sperandio, M. A. Goodale, D. A. Nicolle, B. Rotenberg, N. Duggal, Retinotopic organization of the visual cortex before and after decompression of the optic chiasm in a patient with pituitary macroadenoma. *J. Neurosurg.* **117**, 218–224 (2012).
24. P. J. Basser, D. K. Jones, Diffusion-tensor MRI: Theory, experimental design and data analysis—A technical review. *NMR Biomed.* **15**, 456–467 (2002).
25. S. K. Song, S. W. Sun, W. K. Ju, S. J. Lin, A. H. Cross, A. H. Neufeld, Diffusion tensor imaging detects and differentiates axon and myelin degeneration in mouse optic nerve after retinal ischemia. *Neuroimage* **20**, 1714–1722 (2003).
26. S. K. Song, J. Yoshino, T. Q. Le, S. J. Lin, S. W. Sun, A. H. Cross, R. C. Armstrong, Demyelination increases radial diffusivity in corpus callosum of mouse brain. *Neuroimage* **26**, 132–140 (2005).
27. S. K. Song, S. W. Sun, M. J. Ramsbottom, C. Chang, J. Russell, A. H. Cross, Dysmyelination revealed through MRI as increased radial (but unchanged axial) diffusion of water. *Neuroimage* **17**, 1429–1436 (2002).
28. D. D. Dilks, J. T. Serences, B. J. Rosenau, S. Yantis, M. McCloskey, Human adult cortical reorganization and consequent visual distortion. *J. Neurosci.* **27**, 9585–9594 (2007).
29. B. A. Wandell, S. M. Smirnakis, Plasticity and stability of visual field maps in adult primary visual cortex. *Nat. Rev. Neurosci.* **10**, 873–884 (2009).
30. J. V. Haxby, M. I. Gobbini, M. L. Furey, A. Ishai, J. L. Schouten, P. Pietrini, Distributed and overlapping representations of faces and objects in ventral temporal cortex. *Science* **293**, 2425–2430 (2001).
31. J. Zhang, M. Jones, C. A. DeBoy, D. S. Reich, J. A. Farrell, P. N. Hoffman, J. W. Griffin, K. A. Sheikh, M. I. Miller, S. Mori, P. A. Calabresi, Diffusion tensor magnetic resonance imaging of Wallerian degeneration in rat spinal cord after dorsal root axotomy. *J. Neurosci.* **29**, 3160–3171 (2009).
32. W. Qin, M. Zhang, Y. Piao, D. Guo, Z. Zhu, X. Tian, K. Li, C. Yu, Wallerian degeneration in central nervous system: Dynamic associations between diffusion indices and their underlying pathology. *PLOS One* **7**, e41441 (2012).
33. C. A. Wheeler-Kingshott, M. Cercignani, About "axial" and "radial" diffusivities. *Magn. Reson. Med.* **61**, 1255–1260 (2009).
34. N. Gupta, R. G. Henry, J. Strober, S. M. Kang, D. A. Lim, M. Bucci, E. Caverzasi, L. Gaetano, M. L. Mandelli, T. Ryan, R. Perry, J. Farrell, R. J. Jeremy, M. Ulman, S. L. Huhn, A. J. Barkovich, D. H. Rowitch, Neural stem cell engraftment and myelination in the human brain. *Sci. Transl. Med.* **4**, 155ra137 (2012).
35. D. Le Bihan, J. F. Mangin, C. Poupon, C. A. Clark, S. Pappata, N. Molko, H. Chabriat, Diffusion tensor imaging: Concepts and applications. *J. Magn. Reson. Imaging* **13**, 534–546 (2001).
36. R. T. Naismith, J. Xu, N. T. Tutlam, K. Trinkaus, A. H. Cross, S. K. Song, Radial diffusivity in remote optic neuritis discriminates visual outcomes. *Neurology* **74**, 1702–1710 (2010).
37. H. V. Danesh-Meyer, T. Papchenko, P. J. Savino, A. Law, J. Evans, G. D. Gamble, In vivo retinal nerve fiber layer thickness measured by optical coherence tomography predicts visual recovery after surgery for parachiasmal tumors. *Invest. Ophthalmol. Vis. Sci.* **49**, 1879–1885 (2008).
38. D. N. Parmar, A. Sofat, R. Bowman, J. R. Bartlett, G. E. Holder, Visual prognostic value of the pattern electroretinogram in chiasmal compression. *Br. J. Ophthalmol.* **84**, 1024–1026 (2000).
39. R. J. M. Franklin, C. Ffrench-Constant, Remyelination in the CNS: From biology to therapy. *Nat. Rev. Neurosci.* **9**, 839–855 (2008).
40. S. M. Anstis, Letter: A chart demonstrating variations in acuity with retinal position. *Vision Res.* **14**, 589–592 (1974).
41. S. M. Smith, M. Jenkinson, M. W. Woolrich, C. F. Beckmann, T. E. Behrens, H. Johansen-Berg, P. R. Bannister, M. De Luca, I. Drobnjak, D. E. Flitney, R. K. Niazy, J. Saunders, J. Vickers, Y. Zhang, N. De Stefano, J. M. Brady, P. M. Matthews, Advances in functional and structural MR image analysis and implementation as FSL. *Neuroimage* **23** (Suppl. 1), S208–S219 (2004).
42. T. E. J. Behrens, H. J. Berg, S. Jbabdi, M. F. S. Rushworth, M. W. Woolrich, Probabilistic diffusion tractography with multiple fibre orientations: What can we gain? *Neuroimage* **34**, 144–155 (2007).
43. T. J. Andrews, S. D. Halpern, D. Purves, Correlated size variations in human visual cortex, lateral geniculate nucleus, and optic tract. *J. Neurosci.* **17**, 2859–2868 (1997).
44. G. Gong, T. Jiang, C. Zhu, Y. Zang, F. Wang, S. Xie, J. Xiao, X. Guo, Asymmetry analysis of cingulum based on scale-invariant parameterization by diffusion tensor imaging. *Hum. Brain Mapp.* **24**, 92–98 (2005).
45. J. D. Yeatman, R. F. Dougherty, N. J. Myall, B. A. Wandell, H. M. Feldman, Tract profiles of white matter properties: Automating fiber-tract quantification. *PLOS One* **7**, e49790 (2012).
46. V. Merwade, D. Maidment, B. Hodges, Geospatial representation of river channels. *J. Hydrol. Eng.* **10**, 243–251 (2005).
47. H. H. Dasenbrock, S. A. Smith, A. Ozturk, S. K. Farrell, P. A. Calabresi, D. S. Reich, Diffusion tensor imaging of the optic tracts in multiple sclerosis: Association with retinal thinning and visual disability. *J. Neuroimaging* **21**, e41–e49 (2011).
48. N. Kriegeskorte, W. K. Simmons, P. S. Bellgowan, C. I. Baker, Circular analysis in systems neuroscience: The dangers of double dipping. *Nat. Neurosci.* **12**, 535–540 (2009).
49. D. H. Brainard, The psychophysics toolbox. *Spat. Vis.* **10**, 433–436 (1997).
50. D. G. Pelli, The VideoToolbox software for visual psychophysics: Transforming numbers into movies. *Spat. Vis.* **10**, 437–442 (1997).
51. C. Kupfer, L. Chumbley, J. C. Downer, Quantitative histology of optic nerve, optic tract and lateral geniculate nucleus of man. *J. Anat.* **101**, 393–401 (1967).

Acknowledgments: We are grateful to A. Fintzi and D. Tadin for their contributions to the development of the visual psychophysical tests, and to T. Pasternak, B. Merigan, and P. Shrager for their comments on earlier drafts. **Funding:** This research was supported by National Institute of Neurological Disorders and Stroke grant NS076176 to B.Z.M. and National Eye Institute core grant P30 EY001319 to the Center for Visual Science. D.A.P. was supported by a grant from the University of Rochester Clinical and Translational Science Institute (CTSI TL1 TR000096) and the American Association of Neurological Surgeons Medical Student Summer Research Fellowship. **Author contributions:** D.A.P. planned and carried out the experiments, analyzed the data, generated the figures, and wrote the manuscript. E.G.-C. and G.J.A. carried out the fMRI and psychophysical experiments, respectively, and analyzed the respective data. E.B.H., T.Z., Z.R.W., and G.E.V. planned the experiments and contributed to preparation of the manuscript. T.Z. also assisted with the analysis of the DTI data, and G.E.V. performed all of the transsphenoidal pituitary tumor resections. B.Z.M. planned the experiments, analyzed the data, and wrote the manuscript. **Competing interests:** The authors declare that they have no competing interests. **Data and materials availability:** All data are available upon request from the corresponding author.

Submitted 29 September 2014
Accepted 21 November 2014
Published 10 December 2014
10.1126/scitranslmed.3010798

Citation: D. A. Paul, E. Gaffin-Cahn, E. B. Hintz, G. J. Adeclat, T. Zhu, Z. R. Williams, G. E. Vates, B. Z. Mahon, White matter changes linked to visual recovery after nerve decompression. *Sci. Transl. Med.* **6**, 266ra173 (2014).

Science Translational Medicine
AAAS

White matter changes linked to visual recovery after nerve decompression

David A. Paul *et al.*

Sci Transl Med **6**, 266ra173 (2014);
DOI: 10.1126/scitranslmed.3010798

Editor's Summary

The Healing Brain

In a new study, Paul *et al.* use magnetic resonance imaging in human patients to predict recovery of vision after surgery to remove pituitary gland tumors that have compressed the optic nerve. They found that after tumor removal, the insulation of the nerves regenerated rapidly and that this could be used as a direct marker of vision recovery. This suggests that the brain has a unique ability to heal. A deeper understanding of this healing process could advance treatments for a number of pathologies of the central nervous system involving nerve injury.

Science Translational Medicine (print ISSN 1946-6234; online ISSN 1946-6242) is published weekly, except the last week in December, by the American Association for the Advancement of Science, 1200 New York Avenue NW, Washington, DC 20005.